International Journal of Aeronautical and Space Sciences
https://doi.org/10.1007/s42405-024-00753-1

IJASS International Journal of Aeronautical and Space Sciences

ORIGINAL PAPER

Numerical Study on the Dynamic Behavior of Layered Structures under High-Velocity Impact

Seo Hwee Park[1] · Jin Hyeok Seok[2] · Yeon Su Kim[2] · Yoon A. Kim[2] · Sarath Kumar Sathish Kumar[2] · Taekyung Lee[1] · YunHo Kim[2]

Received: 30 October 2023 / Revised: 22 April 2024 / Accepted: 12 May 2024

Abstract
Spallation occurs when materials exceed their tensile limits under extreme loading conditions, such as high-velocity impacts and shock loading. It is characterized by dynamic void nucleation and fracture growth as tensional waves propagate. Understanding and managing spallation are crucial for maintaining material integrity in extreme circumstances. This study employs numerical methods to investigate spallation and internal pressure in layered structures, which represent the most simplified version of composites. The focus is on understanding the underlying mechanisms and effects of spallation. As the number of layers increases to mimic realistic materials like laminates, the results exhibit behavior similar to that of homogeneous materials, which has significant implications. It is also noteworthy that some layer models of the shock profile, known as the pull-back signal, do not manifest despite the occurrence of internal fractures. This observation suggests that the existing spallation studies on multilayered structures, which rely solely on the shock profile's pull-back signal, may lead to errors in calculating spall strength for composite and layered materials.

Keywords Plate impact simulation · Spallation · Hugoniot elastic limit · Multilayer · Spectrogram

1 Introduction

Spallation is a dynamic nucleation, growth, and coalescence process of void or fracturing during tensile loading [1]. In cases of high-velocity impacts exceeding a few hundred m/s or more, such as ballistic impacts, vehicular crashes, and even micrometeoroid impacts on spacecraft, spallation must be carefully considered when designing protection systems. Spallation is a specific type of dynamic fracture that can lead to fragmentation. The compressive shock waves, which are generated by high-velocity impact, propagate toward the free surfaces of projectile and target. Eventually, the compressive shock waves are reflected as tensile waves from each free surface. Due to the significant differences in impedance between the shocked materials and air, the waves can be reflected on the surface without significant energy loss. However, the reflected waves do not compress but release the materials, forming a rarefactional fan [2–4]. Subsequently, the reflected waves propagate toward the other free surfaces, gradually imposing increasing tensile loading. This can be observed in Fig. 1 at 230 ns and 265 ns. When the dynamic loading from the waves exceeds the critical point of the material, voids can nucleate [5, 6]. As the voids coalesce, multiple cracks form. The formation and extent of cracks, as well as the potential fragmentation of the material, depend on its brittleness and the impact conditions. To observe the damage caused by spallation, a common method is to measure the free surface velocity, known as the shock profile. The shock profile can determine the existence of spallation damage because any wave cannot propagate through a spallation zone. Furthermore, spallation acts as a source for new tensile waves that propagate to each free surface. The formation of spallation cannot be ignored in ballistic application because it can significantly damage the structural integrity of the material [7]. The complicated process of spallation cannot be easily

Communicated by Haeseong Cho.

✉ Taekyung Lee
taeklee@pnu.edu

[1] Metal Design and Manufacturing Lab, School of Mechanical Engineering, Pusan National University, Busan, Republic of Korea

[2] Extreme Environment and Impact Lab, Department of Aerospace Engineering, Seoul National University, Seoul, Republic of Korea

Published online: 19 June 2024

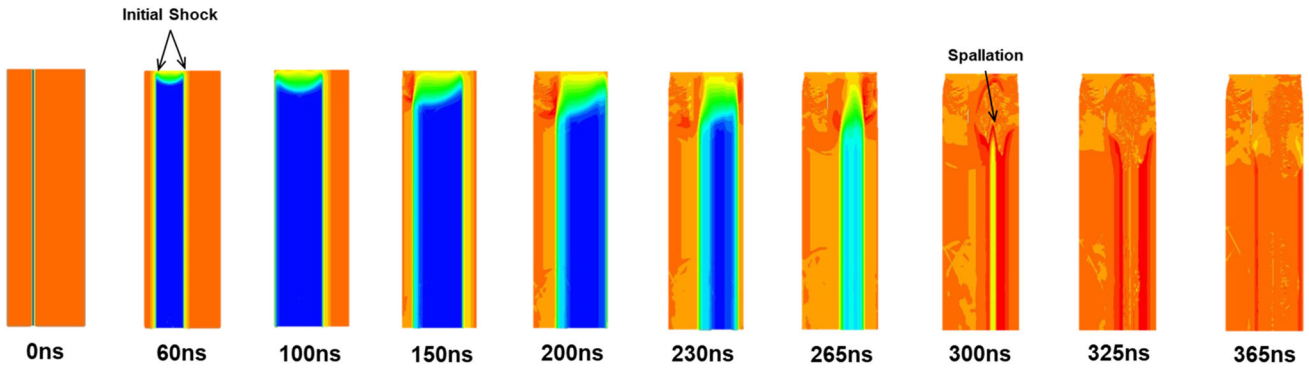

Fig. 1 Homogeneous material impact 2-D simulation internal view

observed and estimated due to its occurrence inside the material, despite its importance. Therefore, numerical methods and postmortem analysis are known to be the only reliable sources for precisely understanding spallation.

In the experiment, there are two main methods: directly irradiating the laser beam on the target [8, 9], or impacting the flyer material on the target, which is a simpler and more basic approach [6, 10, 11]. Cracks generated inside the target can be observed by slicing the target post-experiment [12]. Spall strength can be calculated from the shock profile obtained from a sensor measuring the velocity of the target's surface or a pressure transducer [5, 9–16]. In high-speed impact experiments, several factors affect the accuracy of the results. For high-speed plate impact experiments, precise contact between the plates is crucial for accurate results. However, if the projectile flies at high speed, it may rotate or bend, making ideal surface-to-surface impact almost impossible [17]. This can introduce noise and errors in the shock profile [18, 19]. To minimize these errors and noises, numerical models can be used. For example, [14] demonstrates the nucleation, growth, and coalescence of voids in very small time steps. Additionally, Huang X's model aids in observing the primary incident location and the initial spallation, which are difficult to observe using experimental methods [20].

Composite materials are commonly used in extreme loading situations, such as space environments or bulletproof applications, where the spallation phenomenon must be considered. Due to their superior mechanical properties, extensive experimental and numerical studies on composite materials under high-velocity impact have been conducted [21, 22]. Especially, impact studies on ultrahigh molecular polyethylene (UHMWPE) have been conducted [23–26]. Lässig's model clarified the impact analysis of UHMWPE composite materials and determined the location of spall fractures through the shock profile [23]. This study analyzed the shock profile of the specimen using a gauge on its free surface and examined the location of the spall fracture. Hazell's model analyzed the shock profile through the free surface of the specimen in a plate impact situation [24]. However, no analysis was conducted through the pull-back signal, which is a direct evident mark of spallation damage. Zhang and Ćwik observed delamination and spallation of the laminated specimen due to the shock generated by the initial impact [25]. However, the model mainly focused on residual velocity and did not analyze the shock profile. Research on the impact behavior of carbon fiber-reinforced plastic (CFRP), which is widely used in various fields such as aerospace, was also conducted. [27–30]. Gay et al. studied the behavior of internal shock through data measurement and numerical method [27, 28]. Gilath's model showed the spallation, which is delaminated inside the specimen due to impact [29]. Bie conducted research on the impact behavior of multilayer epoxy and carbon nanotubes (CNTs) [30]. While their studies successfully analyzed shock profiles in the composites, they were limited in their ability to fully explain the material behavior due to their dependency solely on one-dimensional signals from the free surface, thereby excluding the internal dynamic perspective.

The shock wave profile of composite materials is a significant and critical factor that needs to be considered for practical applications. Although composite materials are commonly used in impact applications, understanding the dynamic behavior of composites and multilayer materials is difficult by just experimentally obtaining shock wave profiles. The difference in impedance between the reinforcing material and the matrix material can lead to wave reflection, transmission, and delamination, resulting in unexpected behavior and impact performance. Therefore, to understand internal changes, it is essential to combine the analytical and experimental approaches.

In this study, we simulated high-velocity plate impact on multilayered materials, which are the most simplified composite models meant for understanding how impedance mismatch affects shock and wave propagation. We considered the effect of changing the order of constituent materials, the number of layers, and the corresponding overall thickness of the multilayer target as parameters. Our numerical models revealed that a multilayered material with a sufficient number

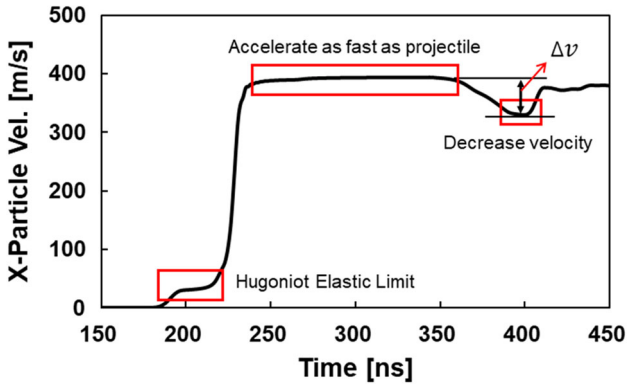

Fig. 2 Shock profile of steel

of layers behaves like a non-composite material in terms of shock and wave propagation, despite the obvious impedance mismatch.

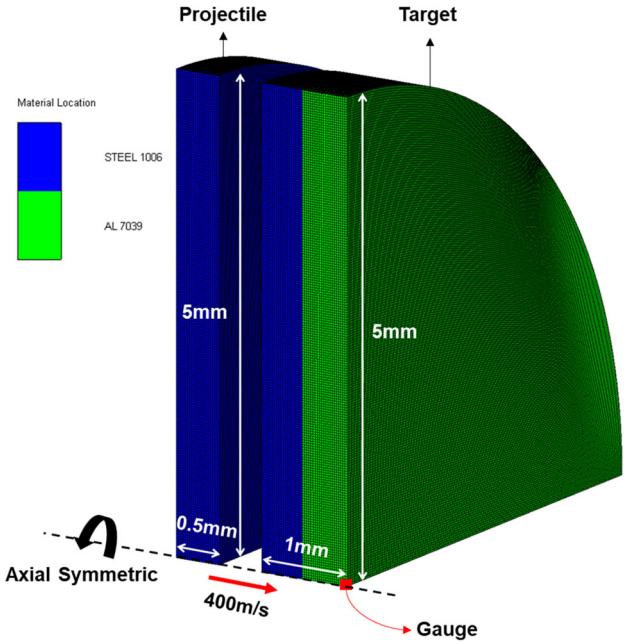

Fig. 3 400m/s impact modeling of [St/Al]

2 Modeling and Method

The spall strength, which varies depending on the physical properties and structural characteristics of materials, is analyzed by measuring the alteration in x-direction velocity obtained by attaching a gauge to the center of the target's free surface, which is a commonly used measurement method in impact tests. Numerical analysis was performed using Ansys-Autodyn. Figure 2 shows the x-direction velocity obtained from the gauge as a graph over time. Spall strength can be calculated using the difference between the section where the speed is kept constant and the speed reduced in the pull-back signal, with the calculation formula given in Eq. (1).

In this research, before analyzing steel–aluminum multilayer models, a homogeneous numerical model of steel-1006, as shown in Fig. 3, was used to optimize the simulation parameters and verify the results. To reduce the number of meshes and simulation time, a 2-D axial symmetric model was implemented. In a model involving a face-to-face impact, the shock wave propagates and reflects off the upper and lower surfaces of the target. To enhance the internal shock wave analysis in this study, adjustments were made to the ratio of target to minimize the influence of shock waves reflected from these surfaces. When the ratio is set to 1:10, the distance from the upper surface to the gauge of the target is approximately 5 mm. Considering the sound speed of the shock inside steel-1006 as 4.569 km/s, the time for the shock to reach the gauge is estimated to be approximately 1100 ns. Consequently, the shock is expected to reach the gauge after the spallation process concludes. The decrease in velocity point where spallation occurs in the shock profile, as shown in Fig. 2, happens at 400 ns; therefore, the geometry interference effect can be reduced.

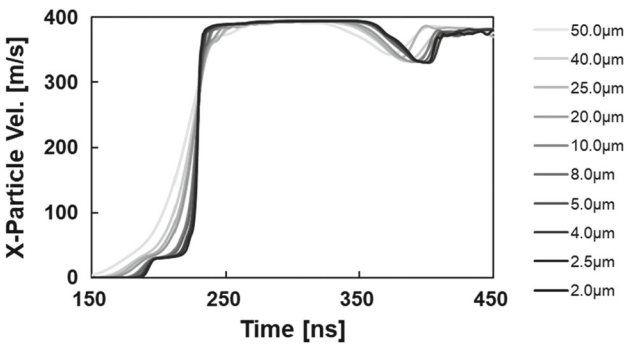

Fig. 4 Shock profile depending on the element size

$$\sigma_{\text{Spall}} = \frac{1}{2}\rho C \Delta v. \tag{1}$$

Furthermore, since the mesh element size can also affect the simulation results, the comparison results of simulations with different sizes can be seen in Fig. 4. As the mesh becomes smaller, it more closely resembles the actual impact behavior, and the accuracy in the result analysis increases. The Hugoniot elastic limit (HEL) can be observed in the gauge after the impact in high-velocity plate impact situations, and as the mesh size decreases, it gradually tends to be consistent. Additionally, the results showed that, as the mesh size decreases in size, the velocity re-acceleration section after the pull-back signal, which indicates spallation, becomes progressively consistent.

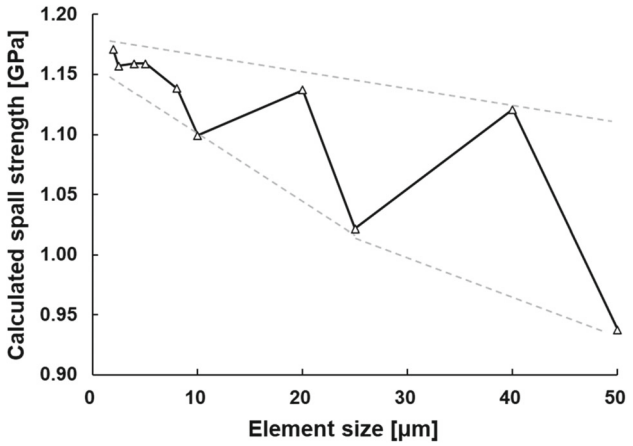

Fig. 5 Calculated spall strength depending on the element size

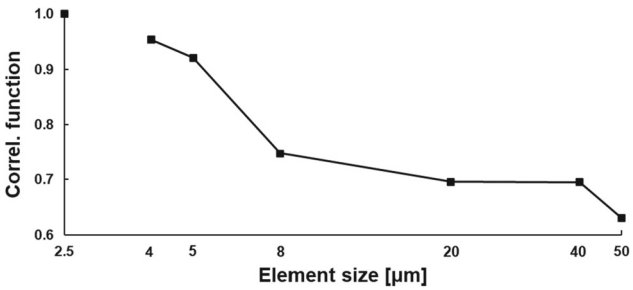

Fig. 6 Comparison of the correlation function with 2.5 μm mesh size

In particular, as the element size increases, as shown in Fig. 5, the calculated spall strength tends to fluctuate. The calculated spall strength value demonstrates an increasing trend as the element size decreases. This phenomenon is attributed to the heightened Δv in Eq. (1). As the element size increases, representing the intricacies of the shock wave becomes challenging. An examination of the HEL point, generated due to the difference in velocity between the elastic and plastic waves reveals a decrease in the representation of detail in larger element size cases compared to smaller cases. As a consequence, the depiction of HEL takes on a distorted shape instead of a plateau. This outcome differs significantly from the idealized result and will impact the shape of the reflected shock wave when calculating spall strength. The phenomenon of decreased precision is consistently observed up to the 360 ns point in the 50 μm case as shown in Fig. 4. This point corresponds to the pull-back signal, which is observed to be generated relatively quickly and decelerates less compared to other element size cases. This occurrence is attributed to the distortion of shock waves and releasing waves caused by the element size. Additionally, the shock profile was compared using the correlation function based on the mesh size of 2.5 μm in Fig. 6. As a result, the 5 μm case exceeding 0.9 was determined to have high reliability and was adopted for modeling. This mesh size was used in the same way for multilayer modeling.

Table 1 Material properties

	Steel	Aluminum
	Shock EOS	
Gruneisen Coefficient	2.17	2
Density	7896 kg/m ^{3}	2770 kg/m^3
C_1	4.569 km/s	5.328 km/s
S_1	1.49	1.338
	Johnson Cook	
Shear modulus	81.8GPa	27.6GPa
Yield stress	350 MPa	337 MPa
Hardening constant	275 MPa	343 MPa
Hardening exponent	0.36	0.41
Strain Rate Constan	0.022	0.01
Thermal Softening Exponent	1	1
Melting temperature	1811 K	877 K
Ref. strain rate	1	1
	Failure - Hydro(Pmin)	
Hydro tensile limit	− 1.01GPa	− 450 MPa
Erosion Strain	3	3

Table 1 shows the material property models of Steel-1006 and Al-7039 used in this research. Spallation is generated as a tension wave progresses in different directions within the material and exceeds the limit of the material. The hydro tension limit of steel and Al was set to − 1.01 GPa and − 450 MPa, respectively.

The validity of the numerical method employed is reinforced by demonstrating the relationship between Us–Up extracted from both the input and analysis results, as seen in Fig. 7. The results conform to the established U_s–U_p relation, $U_s = S_1\, U_p + C_0$. A comparison of the error relative to

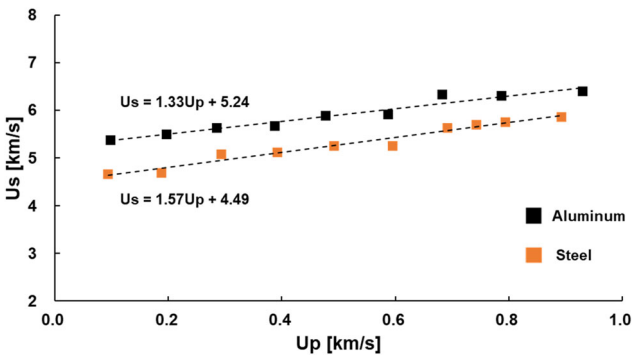

Fig. 7 Relation between the shock velocity and particle velocity for the steel and aluminum model

Table 2 Comparison of the input and analysis results

		Input	Result	Relative error [%]
Steel	Spall strength	1.01 GPa	1.07 GPa	6.03
	S_1	1.49	1.57	5.57
	C_0	4.569 km/s	4.489 km/s	1.76
Aluminum	Spall strength	0.45 GPa	0.43 GPa	5.43
	S_1	1.33	1.33	0.34
	C_0	5.328 km/s	5.239 km/s	1.66

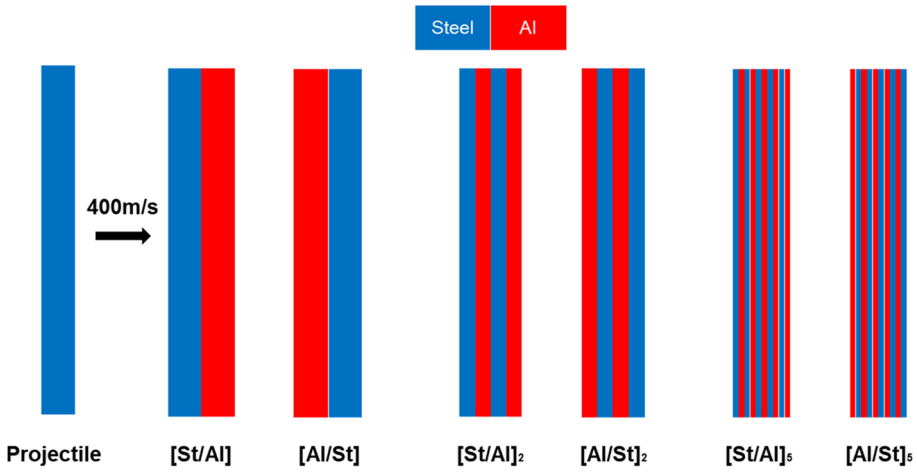

Fig. 8 Impact modeling of the multilayer material

the input is presented in Table 2. Additionally, as illustrated in Fig. 8, the size of the multilayer outline was set to be the same as that of the steel-1006 homogeneous material model. The combination of steel and aluminum is insufficient, but the numerical method assumes an ideal situation. For each layered case, two models were created and compared to observe the effects of the stacking order of the multilayer model. Cases with two, four, and ten layers were modeled to investigate changes in dynamic behavior as the number of layers increased. This was examined using shock profiles and spectrograms. To exclusively analyze the dynamic behavior of the target, the projectile conditions were modeled the same as those in the homogeneous material model. The layer thickness of the two materials used in each model is identical, and the element size is also set to 5 μm.

Table 2 shows a comparison of input and analysis results for verification of the analytical model.

3 Results

3.1 The Homogeneous Model

In the two pure target cases shown in the shock profile and spectrograms of Figs. 9 and 10, ordinary features can be observed. Especially, the HEL and spall strength from the pull-back signal can also be clearly seen in Fig. 9. The case of the aluminum target has more reflections than the other case because of the impedance differences between the target and projectile, as shown in Fig. 10. However, spallation was simulated in both figures. The black lines emphasize the fractured region of the material due to spallation. At the plateau after the shock wave, the free surface velocity of the aluminum target was much higher than that of steel due to the higher sound speed (~ km/s) in the target.

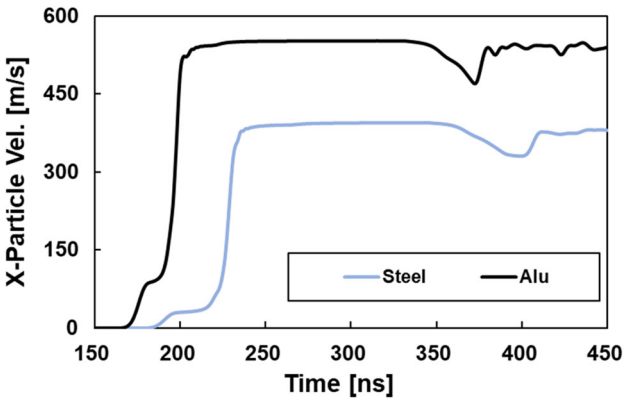

Fig. 9 Homogeneous model shock profile

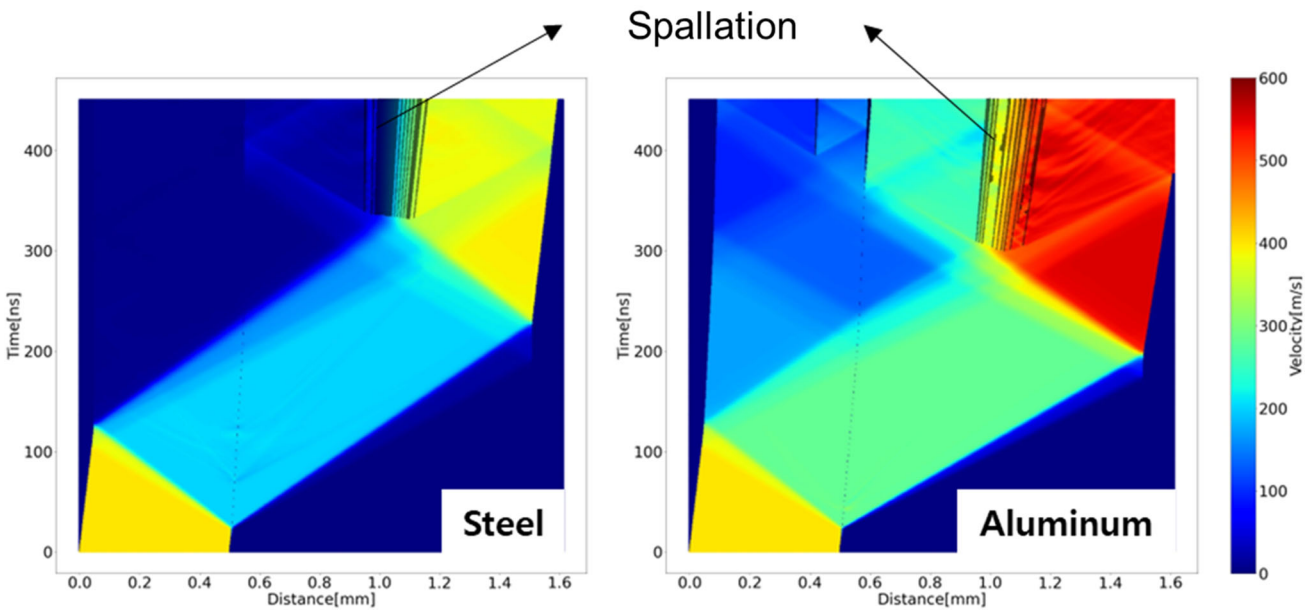

Fig. 10 Shock spectrograms of homogeneous models

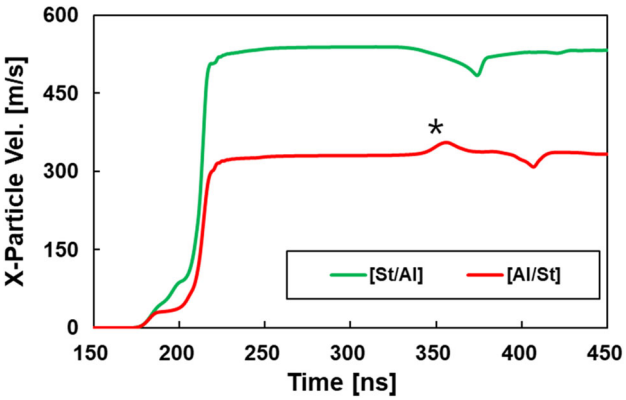

Fig. 11 The two-layer model shock profile *: push-forward signal.

3.2 The Two-Layer Model

The dynamic behavior of heterogeneous targets with two layers exhibits more complex features than that of pure targets. The interface between the layers creates a discontinuous impedance, which causes reflection and transmission, leading to changes in particle velocity before and after the interface. As shown in Fig. 11, the [St/Al] and [Al/St] targets have free surface velocities of 530 m/s and 330 m/s, respectively. The significant difference in free surface velocities demonstrates that the stacking order of two different layers can significantly alter the behavior of materials under shock loading. The different stacking order also influences the internal behavior, as shown in Fig. 12. Immediately after the initial impact, the particle velocity in the first layer was measured as 200 m/s for the [St/Al] model and 280 m/s for the [Al/St] model, as shown by the red arrow, indicating that the [Al/St] model had a higher velocity by 80 m/s in Fig. 12. To satisfy the shock compatibility equation, the first shock waves in the two models have different impedance as well as different particle velocities. The plateau velocity of the free surface is mainly determined by the number of different layers propagated. The [St/Al] target exhibited multiple lines of spallation failure, depicted by vertical black lines, similar to the case of the pure aluminum target, except for earlier spallation lines in the projectile at about 230 ns instead of 300 ns in the pure aluminum target. This trend of early failure is due to the accumulated waves from both reflected waves from both the interface of [St/Al] and the free surface from the projectile. It is interesting to observe that the spallation lines were noticeably postponed from 300 to 400 ns in the [Al/St] target. Furthermore, a push-forward signal, marked with a black star (*) in the [Al/St] model at 350 ns, can be found in Fig. 11 before the pull-back signal appears. In the spectrogram of the [Al/St] target in Fig. 12, the double consequential reflections from the two interfaces sandwiched by two steel materials cause the unique signal before the pull-back signal. These results suggest that simply altering the stacking order of two distinct impedance materials can lead to a complete transformation in both the external and internal material behavior.

3.3 The Four-Layer Model

Compared to the two-layer models, heterogeneous models with four layers indicate a higher level of complexity within

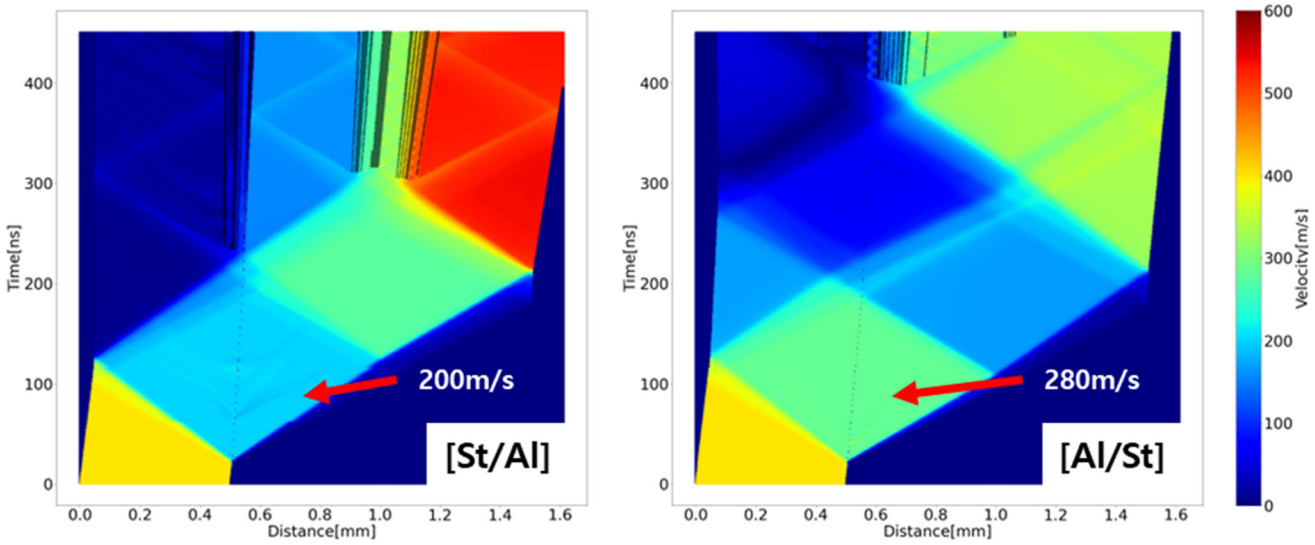

Fig. 12 Shock spectrograms of the two-layer models

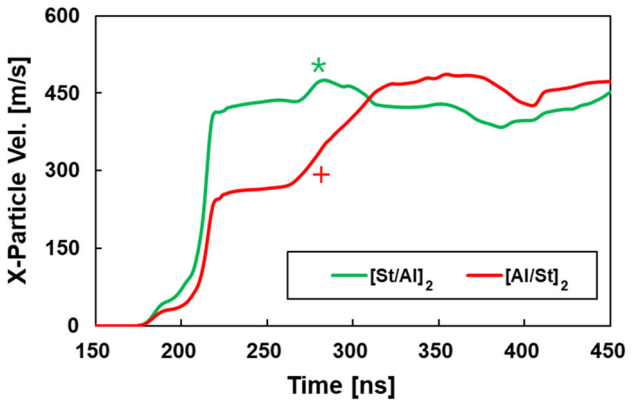

Fig. 13 The four-layer model shock profile *: push-forward signal, + : increase in free surface velocity after the first plateau

the target, primarily due to the increased number of interfaces. This complexity, leading to multiple transmissions, reflections, and super positions, prevents the waves from propagating without a significant loss. Therefore, the free surface plateau velocity can be determined by the number of wave transmissions from the aluminum to steel layer, as observed in the two-layer model. As depicted in Fig. 13, there was a significant difference in the first plateau velocities between the $[St/Al]_2$ and $[Al/St]_2$ models of 430 m/s and 270 m/s, respectively. In the $[St/Al]_2$ model, there is one transmission in the target, while in the $[Al/St]_2$ model, there are two transmissions. Consequently, compared to the $[Al/St]_2$ model, the free surface first plateau velocity is significantly higher in the $[St/Al]_2$ model. This difference in free surface plateau velocity follows a similar trend observed in the two-layer models.

Interestingly, Fig. 13 depicts a distinctive increase in free surface particle velocity at 260 ns in the $[Al/St]_2$ model after the first plateau. This increase can be attributed to the abrupt change in impedance at the many interfaces, leading to reflection, transmission, and superpositions of shock waves within the $[Al/St]_2$ target. In detail, all the shock waves originating at numerous interfaces accelerate the particles rightward, leading to establishment of a strong shock wave in the last layer at 260 ns, as remarked with red cross (+) in the $[Al/St]_2$ model of Fig. 14.

The "push-forward" signal marked with green star (*) and internal failure in the projectile can be observed only in the cases where steel is the first layer. Internal failure of the projectile primarily occurs when the shock wave is reflected at the first interface in the target and propagated into the projectile. Additionally, the failure location in the projectile differs from that observed in the [St/Al] model. In $[St/Al]_2$, the failed region is near the center of the projectile. However, failure occurs near the interface between the projectile and target of [St/Al]. This difference is attributed to the thickness of the target's layers. If the time taken for the shock wave to reach the first interface in the $[St/Al]_2$ model is short, it leads to an earlier reflection compared to that of [St/Al]. Owing to this difference, the reflected shock wave propagates inside the projectile. These distinctions result from shock wave reflections at the first interface of the target, emphasizing the significant influence of material arrangement on dynamic behavior.

3.4 The Ten-Layer Model

The shock profile of heterogeneous models with ten layers shows a decrease in the influence of material arrangement

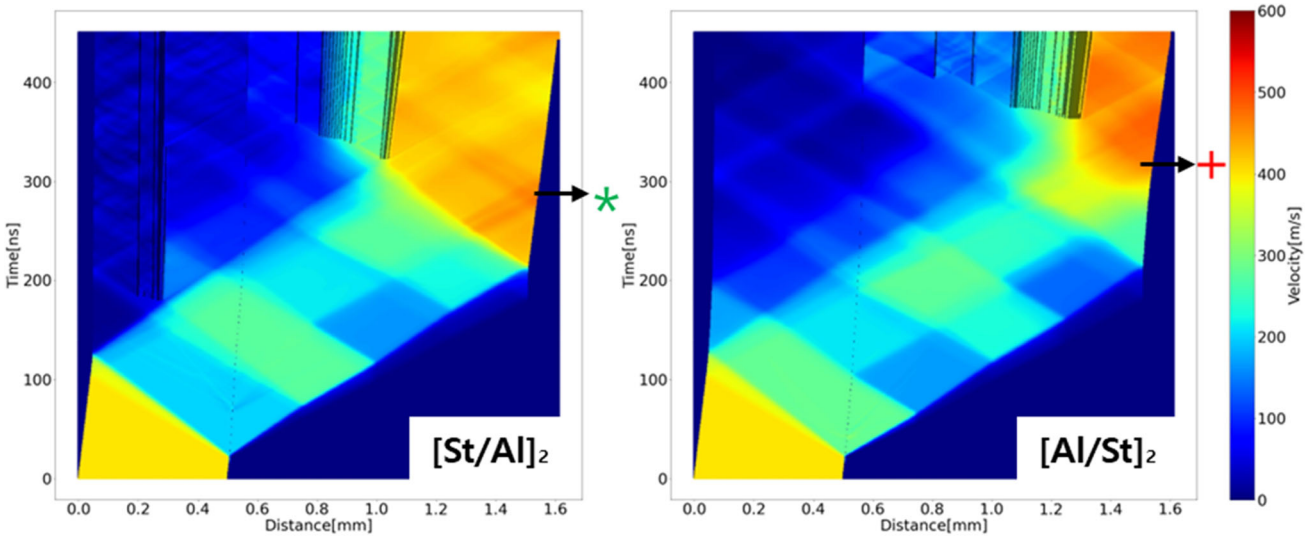

Fig. 14 Shock spectrograms of four-layer models *: push-forward signal, + : increase in free surface velocity after the first plateau

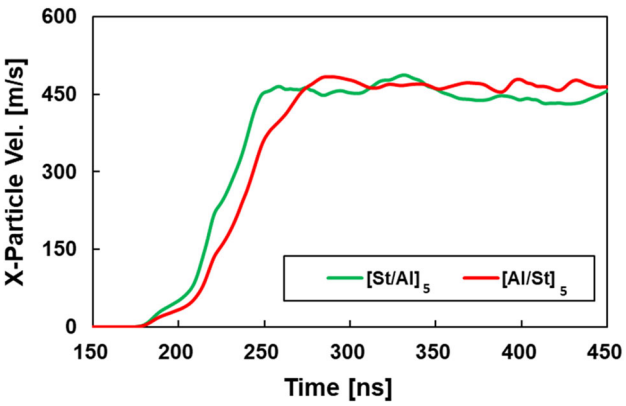

Fig. 15 The ten-layer model shock profile

on dynamic behavior, contrasting with the behavior of the previously studied two-layer and four-layer models. This is illustrated in Fig. 15. Specifically, $[St/Al]_5$ does not exhibit the push-forward signal typical of targets with steel as the first layer, while $[Al/St]_5$ lacks the re-acceleration phase seen in the shock profile of $[Al/St]_2$. Additionally, for both $[St/Al]_5$ and $[Al/St]_5$, the free surface plateau velocity remains consistently at 450 m/s, in contrast to the two-layer and four-layer models where the velocity varied based on material arrangement. Furthermore, in the shock profiles of all heterogeneous models, targets with steel as the first layer tend to show particles accelerating earlier compared to targets with aluminum as the first layer.

With an increase in the number of layers, the influence of the material arrangement order within the target is neutralized. This effect can also be observed inside the target, as shown in the spectrogram in Fig. 16. Notably, in both the models, the spallation inside the target occurs at the same location and time. Specifically, the shock acceleration patterns are very similar, and failures were observed only in the aluminum layer, which has a relatively lower tensile limit, with two clusters of lines. Additionally, a common feature in targets where steel is located as the first layer is the observation of failure within the projectile. This is attributed to the lesser thickness of a layer, considering the location of failure in fewer layers. While the two-layer and four-layer models exhibit variations in the location and timing of spallation depending on the arrangement order, the increase in layers leads to a reduction in these differences, indicating a more uniform behavior. These results suggest that despite the change in arrangement order as the number of layers increased, the propagation of cracks within the target was similar, as was the initial fracture onset. This indicates that the target behaves as if it were composed of a homogeneous material.

4 Discussion

In this study, we numerically demonstrate the features of material arrangement becoming indistinguishable with the increase in the number of layers. As shown in Fig. 17, we compare the similarity of material arrangement based on the number of layers in the shock profiles. As the number of layers increases, the correlation function method, represented by the black line, exhibits a *V*-shape pattern rather than a sequential increase. The correlation results are high for the two-layer case, but relatively low for the four-layer case. This difference arises from the comparison method of the correlation function, which yields higher values when the shape

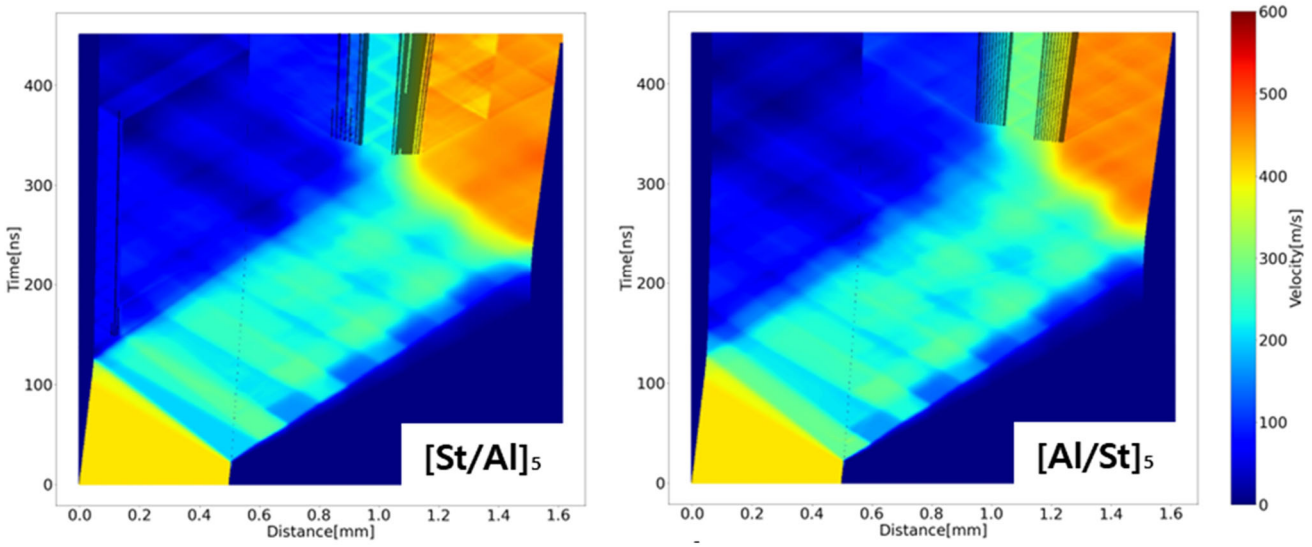

Fig. 16 Shock spectrograms of ten-layer models

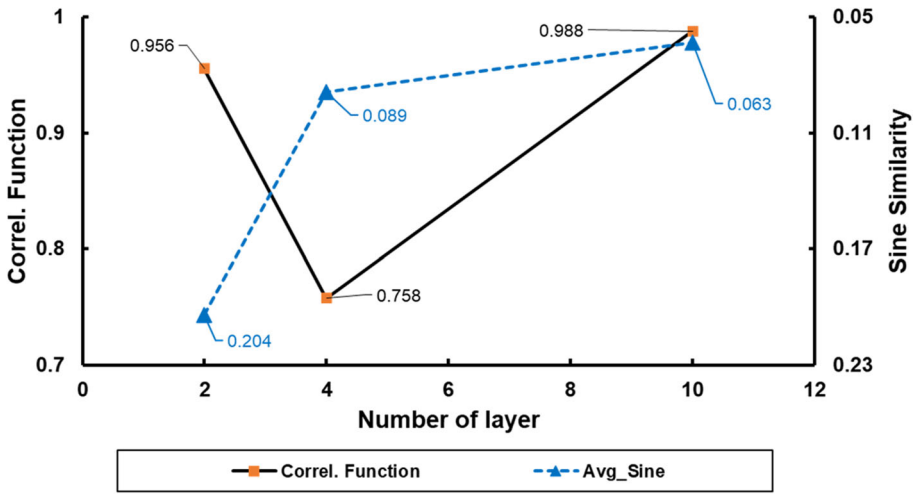

Fig. 17 Similarity of the shock profile

and trend of the graph are similar. For instance, the correlation between $y = x$ and $y = 3 \times$ yields a correlation value of 1. Therefore, the high similarity in the correlation comparison of the two-layer case can be attributed to the similar plateau velocity maintenance time, regardless of the material arrangement and absence of additional acceleration or deceleration regions. Similarly, the difference in the four-layer case arises from the additional acceleration region at 260 ns in the $[Al/St]_2$ model. The "Sine similarity" method compares the angles of the shock profiles in each model. The blue line shown in Fig. 17 represents the "Sine similarity", as shown in Appendix A-1, indicating that, as the number of layers in the target increases, the points increase, and the influence of material arrangement decreases. Through this approach, we observe that the influence of material arrangement diminishes as the number of layers increases, eventually exhibiting dynamic behavior similar to that of the homogeneous material, regardless of the order of the layering material.

Furthermore, compared to other layered structure models, the shock profile and spectrogram of the ten-layer model exhibit distinct features. As shown in Fig. 16, the spectrogram clearly indicates spallation with the presence of black shading. However, as seen in Fig. 14, the indicator of spallation, the pull-back signal, is not observed, although the free surface plateau velocity is visible in the shock profile. This occurs because the shock reflected from the free surface of the projectile, which accelerates toward the left direction, propagates the target interface multiple times. Notably, the measurement of spall strength, which shows the pressure generated during spallation, is based on the pull-back signal. However, for layered structure targets, there is a high possibility of inaccurate measurement of the pull-back signal.

Therefore, we concluded that the spallation research on commonly used materials such as CFRP and UHMWPE may be inaccurate.

5 Conclusion

The shock profile is an exclusively experimental method and has limitations in impact studies. The shock wave propagation within the material can be observed with the spectrogram used in this study. This approach revealed two essential insights into understanding layered materials and composites. Firstly, the stacking order of the two materials used in the target was neglected as the number of layers increased, resulting in dynamic behavior similar to that of a homogeneous material. Secondly, as the number of layers increases, spallation occurs without any corresponding failure signal, commonly referred to as the pull-back signal.

Numerical results of the study suggest that the pull-back signal, which typically serves as an indicator of spallation in experiments, can be easily compromised at the boundary of the multilayer structure. Notably, relying solely on the shock profile obtained by placing the gauge on the free surface of the target in a high-velocity impact situation with a multilayer structure or composites can lead to errors. Therefore, it is suggested that the conventional shock profile method at the free surface of the target may introduce inaccuracies when determining the impact-related properties of advanced heterogeneous materials, including fiber-reinforced composites, under extreme loading conditions such as high-velocity impact, ballistic events, and explosions.

Appendix A

A-1. Sine Similarity Method

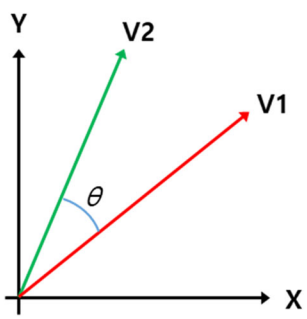

Sine similarity is a method that compares the angular difference between two points simultaneously. Since it measures similarity by comparing the angular, a smaller theta value indicates a higher level of similarity.

$$\text{Similarity}(V_1,\ V_2) = \frac{V_1 \bullet V_2}{\|V_1\| \bullet \|V_2\|}.$$

A-2. Impedance mismatch

$$\psi_r = \frac{Z_1 - Z_2}{Z_1 + Z_2}\psi_i,\ \psi_t = \frac{2Z_1}{Z_1 + Z_2}\psi_i. \tag{2}$$

For shock wave propagation at an interface, ψ_r represents the reflected shock and ψ_t represents the transmitted shock. Z_1 and Z_2 are the impedances of the material through which the shock propagates.

Acknowledgements This work was supported by the Research Institute of Mechanical Technology R&D project (PNU RIMT2022-02), Pusan National University.

Funding The funding has been received from Pusan National University with Grant no. PNU RIMT2022-02.

Declarations

Conflict of Interest The authors declare that they have no known competing financial interests or personal relationships that could have appeared to influence the work reported in this paper.

References

1. Chen X, Asay JR, Dwivedi SK, Field DP (2006) Spall behavior of aluminum with varying microstructures. J Appl Phys. https://doi.org/10.1063/1.2165409
2. Zoppou C, Roberts S (2003) Explicit schemes for dam-break simulations. J Hydraul Eng 129:11–34. https://doi.org/10.1061/(asce)0733-9429(2003)129:1(11)
3. Lee J, Kim YS, Baek SJ, Jeong HS (2021) Study of separation mechanism and characteristics of ridge-cut explosive bolts using numerical analysis. Int J Aeronaut Space Sci 22:84–93. https://doi.org/10.1007/s42405-020-00334-y
4. Cardall CY, Budiardja RD, Endeve E, Mezzacappa A (2012) GenASiS: general astrophysical simulation system. I. Fundamentals. Astrophys J Suppl Ser: 1–55
5. Dynamic Behavior of Materials (1994) Meyers n.d.
6. Hanim S, Klepaczko JR (1999) Numerical study of spalling in an aluminum alloy 7020–T6. Int J Impact Eng 22:649–673. https://doi.org/10.1016/S0734-743X(99)00023-8
7. Li J, Hao H (2014) Numerical study of concrete spall damage to blast loads. Int J Impact Eng 68:41–55. https://doi.org/10.1016/j.ijimpeng.2014.02.001
8. Eliezer S, Gilath I, Bar-Noy T (1990) Laser-induced spall in metals: experiment and simulation. J Appl Phys 67:715–724. https://doi.org/10.1063/1.345777
9. Lescoute E, De Rességuier T, Chevalier JM, Loison D, Cuq-Lelandais JP, Boustie M et al (2010) Ejection of spalled layers from laser shock-loaded metals. J Appl Phys. https://doi.org/10.1063/1.3500317

10. Yuan F, Tsai L, Prakash V, Rajendran AM, Dandekar DP (2007) Spall strength of glass fiber reinforced polymer composites. Int J Solids Struct 44:7731–7747. https://doi.org/10.1016/j.ijsolstr.2007.05.007
11. Jones DR, Fensin SJ, Morrow BM, Martinez DT, Hixson RS (2020) Shock recompaction of spall damage. J Appl Phys. https://doi.org/10.1063/5.0011337
12. Yu Y, Chen D, Tan H, Wang H, Xie S, Zhang M (2007) Spall investigations for LY12 Al using triangular waves. Int J Impact Eng 34:395–404. https://doi.org/10.1016/j.ijimpeng.2005.11.006
13. Schuler H, Mayrhofer C, Thoma K (2006) Spall experiments for the measurement of the tensile strength and fracture energy of concrete at high strain rates. Int J Impact Eng 32:1635–1650. https://doi.org/10.1016/j.ijimpeng.2005.01.010
14. Ren B, Li S, Qian J, Zeng X (2011) Meshfree simulations of spall fracture. Comput Methods Appl Mech Eng 200:797–811. https://doi.org/10.1016/j.cma.2010.10.003
15. Krivtsov AM (1999) Relation between spall strength and mesoparticle velocity dispersion. Int J Impact Eng 23:477–487. https://doi.org/10.1016/s0734-743x(99)00097-4
16. Ikkurthi VR, Chaturvedi S (2004) Use of different damage models for simulating impact-driven spallation in metal plates. Int J Impact Eng 30:275–301. https://doi.org/10.1016/S0734-743X(03)00070-8
17. Chizari M, Barrett LM (2009) Single and double plate impact welding: experimental and numerical simulation. Comput Mater Sci 46:828–833. https://doi.org/10.1016/j.commatsci.2009.04.018
18. Zhu L, Cai W, Chen M, Tian Y, Bi L (2020) Experimental and numerical analyses of elastic-plastic responses of ship plates under ice floe impacts. Ocean Eng 218:108174. https://doi.org/10.1016/j.oceaneng.2020.108174
19. Wang F, Glimm JG, Grove JW, Plohr BJ, Sharp DH (1993) A conservative eulerian numerical scheme for elastoplasticity and application to plate impact problems. IMPACT Comput Sci Eng 5:285–308. https://doi.org/10.1006/icse.1993.1013
20. Huang X, Ling Z, Dai LH (2014) Ductile-to-brittle transition in spallation of metallic glasses. J Appl Phys. https://doi.org/10.1063/1.4897552
21. Kim YH, Moon JB, Cha JH, Kim CG (2020) Stacking order effect of hybrid bumper against high-velocity impact. Int J Aeronaut Space Sci 21:95–104. https://doi.org/10.1007/s42405-019-00189-y
22. Yang JS, Choi MK, Kim CG (2023) Numerical prediction of the impact fracture of a projectile through oblique target. Int J Aeronaut Space Sci. 24:798–811. https://doi.org/10.1007/s42405-023-00620-5
23. Lässig T, Bagusat F, Pfändler S, Gulde M, Heunoske D, Osterholz J et al (2017) Investigations on the spall and delamination behavior of UHMWPE composites. Compos Struct 182:590–597. https://doi.org/10.1016/j.compstruct.2017.09.031
24. Hazell PJ, Appleby-Thomas GJ, Trinquant X, Chapman DJ (2011) In-fiber shock propagation in Dyneema®. J Appl Phys. https://doi.org/10.1063/1.3622294
25. Zhang R, Qiang LS, Han B, Zhao ZY, Zhang QC, Ni CY et al (2020) Ballistic performance of UHMWPE laminated plates and UHMWPE encapsulated aluminum structures: numerical simulation. Compos Struct 252:112686. https://doi.org/10.1016/j.compstruct.2020.112686
26. Ćwik TK, Iannucci L, Curtis P, Pope D (2016) Investigation of the ballistic performance of ultra high molecular weight polyethylene composite panels. Comp Struct 149:197–212. https://doi.org/10.1016/j.compstruct.2015.11.009
27. Gay E, Berthe L, Buzaud E, Boustie M, Arrigoni M (2013) Shock adhesion test for composite bonded assembly using a high pulsed power generator. J Appl Phys. https://doi.org/10.1063/1.4811696
28. Gay E, Berthe L, Boustie M, Arrigoni M, Buzaud E (2014) Effects of the shock duration on the response of CFRP composite laminates. J Phys D Appl Phys. https://doi.org/10.1088/0022-3727/47/45/455303
29. Gilath I, Eliezer S, Shkolnik S (1990) Spall behaviour of carbon epoxy unidirectional composites as compared to aluminum and iron. J Compos Mater 24:1138–1151. https://doi.org/10.1177/002199839002401102
30. Bie BX, Han JH, Lu L, Zhou XM, Qi ML, Zhang Z et al (2015) Dynamic fracture of carbon nanotube/epoxy composites under high strain-rate loading. Compos Part A Appl Sci Manuf 68:282–288. https://doi.org/10.1016/j.compositesa.2014.10.001